

Generation of amorphous Si structurally compatible with experimental samples through the quenching process: a systematic molecular dynamics simulation study

Iván Santos^{a,*}, María Aboy^a, Luis A. Marqués^a, Pedro López^a, Lourdes Pelaz^a

^a*Departamento de Electricidad y Electrónica, E.T.S.I. de Telecomunicación, Universidad de Valladolid, Paseo Belén 15, 47011 Valladolid, Spain*

Abstract

The construction of realistic atomistic models for amorphous solids is complicated by the fact that they do not have a unique structure. Among the different computational procedures available for this purpose, the melting and rapid quenching process using molecular dynamics simulations is commonly employed as it is simple and physically based. Nevertheless, the cooling rate used during quenching strongly affects the reliability of generated samples, as fast cooling rates result in unrealistic atomistic models. In this study, we have determined the conditions to be fulfilled when simulating the quenching process with molecular dynamics for obtaining amorphous Si (*a*-Si) atomistic models structurally compatible with experimental samples. We have analyzed the structure of samples generated with cooling rates ranging from $3.3 \cdot 10^{10}$ to $8.5 \cdot 10^{14}$ K/s. The obtained results were compared with experimental data available in the literature, and with samples generated by other state-of-the-art and more sophisticated computational procedures. For cooling rates below 10^{11} K/s, *a*-Si samples generated had structural parameters within the range of experimental samples, and comparable to those obtained from other refined modeling procedures. These computationally slow cooling rates are of the same order of magnitude than those experimentally achieved with pulsed energy melting techniques. Samples obtained with faster cooling rates can be further relaxed with annealing simulations, resulting in structural parameters within the range of experimental samples. Nevertheless, the required annealing times are on the order of microseconds, which makes this annealing step non practical from a computational point of view.

Keywords: Amorphous silicon, quenching process, molecular dynamics simulations, atomistic structure

*Corresponding author

Email address: ivasan@tel.uva.es (Iván Santos)

1. Introduction

Amorphous silicon (*a*-Si) is a material of great interest for state-of-the-art inexpensive high efficient heterojunction and thin-film solar cells [1]. *a*-Si also plays an important role for junction formation in electronic devices as solid phase epitaxial regrowth of *a*-Si results in high dopant activation [2, 3]. There is a variety of experimental procedures for *a*-Si generation [4–6]. Some methods consist in the deposition of a vapor containing Si atoms on a convenient substrate. The vapor can be obtained from the evaporation or sputtering of a solid Si source (physical vapor deposition, PVD) [5, 7], or from the decomposition of precursor Si gases (chemical vapor deposition, CVD) by pyrolysis or glow-discharge (plasma-enhanced) [5, 8]. Evaporation and sputtering processes are generally considered to have cooling rates on the order of 10^8 K/s [4]. Other methods to produce *a*-Si consist in the direct modification of a crystalline Si (*c*-Si) substrate. Ion, electron and neutron irradiation of *c*-Si induce *a*-Si formation by the accumulation of radiation induced damage [5, 9–13]. Indentation can also promote *a*-Si through a pressure induced phase transformation [5, 13]. *a*-Si can also be generated by quenching liquid Si (*l*-Si). Bulk-quenching methods are limited to cooling rates of less than $10^7 - 10^8$ K/s, while pulsed energy quenching processes have typical cooling rates of $\gtrsim 10^{10}$ K/s [4, 6]. Only these fast cooling rates from pulsed energy melting techniques can prevent Si crystallization during the quenching process of *l*-Si [4–6, 14–17].

All these experimental procedures result in *a*-Si samples with different properties and defect concentrations [5, 18]. Defects present in *a*-Si interact with charge carriers [19, 20], affect dopant diffusion [21] and limit the efficiency of fabricated devices [22]. Experimentally observed defects in *a*-Si are associated to non four-fold coordinated Si atoms (like dangling or floating bonds, which are three- and five-folded Si atoms, respectively) or highly stretched Si-Si bonds in the material [23]. *a*-Si samples generated by CVD present an electron spin resonance signal much smaller than those generated by PVD [18, 24], which is related to a lower density of dangling bonds. Samples obtained by laser quenching resulted in structural characteristics similar to those obtained by CVD [5, 15, 17], and are compatible with well relaxed *a*-Si [5]. PVD, irradiation and indentation processes generate unrelaxed *a*-Si samples [5, 13], which are commonly treated with subsequent thermal annealings to reduce the defect density [5, 9–13].

The inherent variability of the *a*-Si configuration and properties depending on the fabrication process make the proper modeling of its structure difficult. An adequate understanding of the amorphous structure is needed, and recent studies demonstrate the interest in providing realistic atomistic models of amorphous solids that reproduce the structure of experimental samples [25–29]. *a*-Si has been considered as a prototype for tetrahedrally coordinated covalent amorphous materials, which can be described as a continuous random network (CRN) [6, 30]. CRN structural models consist of a network of atoms assembled at random positions with the

sole restriction that each atom must be perfectly coordinated according to its valence. For this purpose, small deviations from the crystalline bond angle and bond length are allowed. Despite the simplicity of this idea, its practical realization is not straightforward. The first algorithm to construct a CRN structure for covalent amorphous materials was developed by Wooten, Winer and Weaire, the so-called WWW algorithm [31]. It starts from the crystalline structure, and it introduces local bond rearrangements in the lattice while keeping the four-fold coordination of Si atoms. Barkema and Mousseau (BM) optimized the WWW algorithm [32, 33] and removed the restriction of starting from a crystalline structure while their algorithm also forces four-fold coordination. Both the WWW and the BM procedures result in *a*-Si samples where all atoms are four-fold coordinated, and thus satisfying the principle of the CRN model, but intrinsic defects present in experimental samples are not reproduced. Neither the algorithms used in WWW and BM procedures are based on any physical process nor experimental data is used as reference during the generation of the *a*-Si samples. Nevertheless the pair correlation function (PCF) of generated samples agree very well with experimental results [31–33]. A similar procedure to WWW and BM consists on the accumulation of bond defects in *c*-Si [34–36]. Bond defects are local rearrangements of bonds in the Si lattice with no excess or deficit of atoms and keeping the four-fold coordination of atoms. This defect can result from a pure ballistic process or by incomplete Si interstitial-vacancy recombination, and it has been used for modeling ion-beam-induced amorphization and recrystallization of *c*-Si [34, 35]. *a*-Si samples generated by the accumulation of bond defects have large concentration of coordination defects as the desired concentration of bond defects is first introduced in the simulation cell and then the resulting configuration is relaxed [36], while in WWW and BM models relaxation is performed after each bond rearrangement.

A different theoretical procedure for obtaining structural models of *a*-Si consist in using sophisticated reverse Monte Carlo (RMC) techniques. These techniques create atomistic models by fitting their structure factor and PCF to available diffraction data from experiments [37–40]. RMC techniques are not based on any physical process, but experimental data is used as reference. Thus, they reproduce the experimental data used in the fitting process, but they are not predictive. Structures obtained using RMC techniques can present coordination defects rather than perfect four-fold coordination as in WWW and BM models. Initial RMC algorithms resulted in quite unrealistic bond angle distributions, large bond angle deviations, and large concentration of coordination defects [25, 28, 38]. More recently, RMC algorithms have been improved by including interatomic forces from empirical potentials or *ab initio* calculations in the fitting procedure that lead to more realistic atomistic models [25–28, 41].

Paracrystalline atomistic models have also been proposed for describing the atomic structure of *a*-Si [42–46].

These models have shown to adequately describe the experimental PCF and structure factor of *a*-Si, as well as fluctuation electron microscopy data. These models are made computationally by inserting randomly oriented nanometric *c*-Si grains in an amorphous matrix, followed by energy minimizations of the configurational energy.

There are also computational procedures for generating *a*-Si using molecular dynamics (MD) simulations that resembles some physical processes. One example is the generation of *a*-Si through the accumulation of damage generated by energetic atoms, which resembles the generation of *a*-Si by ion irradiation. Nevertheless, this procedure results in atomistic models with large concentration of coordination defects *a*-Si [13, 36]. Another common and simpler procedure for generating *a*-Si using MD simulations is by the quenching of *l*-Si [13, 27, 47–50], which resembles the preparation of *a*-Si by pulsed energy melting techniques. Typical cooling rates used in this computational procedure are of the order of $10^{13} - 10^{14}$ K/s [13, 27, 47, 48], while few studies have characterized samples generated with slower cooling rates [49–51]. These cooling rates are comparable (and some of them larger) to cooling rates experimentally achieved in pulsed energy melting techniques [4, 6]. The cooling rate considered in the simulation severely limits the reliability of generated *a*-Si structures, as unrealistic fast cooling rate results in *a*-Si samples with a large concentration of coordination defects. This is the main argument against the use of quenching process for obtaining *a*-Si through computer simulations [13, 27].

In the present work we focused on the quenching process using MD simulations for generating atomistic models of *a*-Si as it is a physically based and simple method that can be easily implemented. As previously indicated, this procedure has been extensively used in the past. Nevertheless, cooling rates achieved were highly limited by the available computational resources, and not so well relaxed *a*-Si samples were generated. Nowadays, high performance computing facilities have removed this limitation and slower cooling rates are possible. The aim of this work is to review the features of *a*-Si samples generated by quenching process using MD simulations in order to determine the conditions that have to be fulfilled for obtaining *a*-Si atomistic models with structural parameters comparable with experimental samples. For this purpose, we used a wide range of cooling rates, and we analyzed the structure of generated samples in terms of bond lengths and bond angle deviations. We first verified that trends found in other works using the quenching process are also satisfied by samples generated in the present work. We then compared their structural parameters with data of different types of *a*-Si from experiments and other computational works available in the literature. This comparison served us to establish the range of cooling rates that resulted in *a*-Si models structurally compatible with experimental samples. We also analyzed the feasibility of subsequent thermal annealings for effectively relaxing *a*-Si samples generated by relatively fast cooling rates within the range of structural parameters of experimental samples.

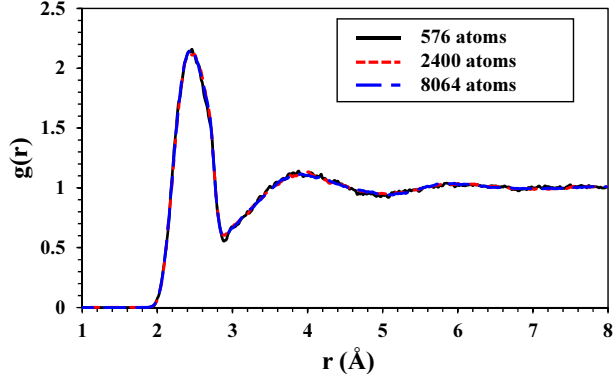


Figure 1: Pair correlation function of samples after equilibration at 4000 K during 3 ps.

2. Simulation details

We used the Tersoff potential in its third parametrization to describe the Si-Si interactions in our simulations [52]. This empirical potential has been shown to properly describe atomic structures different from the tetrahedral bonding of the zinc-blende lattice. For example, it was successfully used to study the structure of point defects [53] and extended defects [54, 55] in *c*-Si, the Si amorphous phase [56], and the crystal growth from the amorphous [57] and the liquid [58] phase. We used for all the simulations an in-house MD simulation code that has been extensively used in previous works [34–36, 53, 56].

The starting atomistic configuration of our simulations was a simulation cell of *c*-Si in the zinc-blende structure. This simulation cell was bounded by (1 0 0) planes in the X direction and by (1 1 0) planes in Y and Z directions, and we applied periodic boundary conditions in all spatial directions. We used a lattice parameter of $a_0 = 5.43 \text{ \AA}$, and three different sizes for the simulation cells: $4a_0 \times 6\sqrt{2}a_0 \times 6\sqrt{2}a_0$ (with 576 atoms), $6a_0 \times 10\sqrt{2}a_0 \times 10\sqrt{2}a_0$ (with 2400 atoms), and $9a_0 \times 13\sqrt{2}a_0 \times 13\sqrt{2}a_0$ (with 6084 atoms).

To generate *a*-Si samples by the quenching process, we first melted these *c*-Si simulation cells by heating them to 4000 K and equilibrating them at this temperature during 3 ps. We represented the PCF of samples at the end of the equilibration phase in Fig. 1. It can be seen that the curves are identical for the three system sizes, and they agree with the PCF of *l*-Si described by Tersoff empirical potential [52, 56, 59]. Figure 1 indicates that no signatures of the initial crystalline state are left after the equilibration at 4000 K. The same PCF is also obtained after 34 ps and 65 ps equilibration at 4000 K for all system sizes (not shown), which indicates that the liquid is properly equilibrated after 3 ps.

After the equilibration step at 4000 K, simulation cells were quenched to 300 K using cooling rates ranging

from $3.3 \cdot 10^{10}$ to $8.5 \cdot 10^{14}$ K/s by removing kinetic energy every a given number of time steps, and letting the system evolve through the NVE ensemble between energy removals. The amount of kinetic energy removed and the number of time steps between energy removals determined the cooling rates of the simulation. Crystallization occurred for cooling rates slower than $3.3 \cdot 10^{10}$ K/s. Finally, as-quenched samples were thermalized at 300 K during 10 ps, and atomic positions, kinetic and potential energies were averaged during the last 5 ps for obtaining the potential energy of the amorphous structure (evaluated as the difference between the averaged potential and kinetic energies) with respect to *c*-Si at 300 K, the PCF, the atomic coordination (from the integral of the nearest neighbor peak of the PCF), and the bond length and angle distributions using a nearest-neighbor bonding cutoff of 2.85 Å.

Some of the *a*-Si samples were used as the initial configuration for annealing simulations at temperatures from 900 K to 1300 K during times ranging from 0.95 to 0.75 μ s, with shorter simulation times corresponding to higher annealing temperatures. We averaged the kinetic and potential energies during simulations every 1000 steps to visualize the relaxation of the samples. These simulations were intended to analyze the effect of the annealing process on the structural characteristics. The final atomic structure resulting from the annealing simulation was thermalized at 300 K for evaluating their energetic and structural characteristics. We considered in all our simulations a time step of 1 fs.

3. Results and discussion

We represented in Fig. 2 the energetic and structural characteristics of obtained *a*-Si samples as a function of the cooling rate. As the cooling rate is slower, the potential energy is reduced, the averaged structural features are closer to those of *c*-Si (atomic coordination approaches four, bond length and angle are closer to $r_0 = 2.35$ Å and $\theta_0 = 109.47^\circ$), and the bond angle ($\Delta\theta$) and length ($\Delta\sigma$) deviations are reduced [49]. It can be seen that there is an excellent agreement between the results obtained with the different system sizes, so we will focus on the results obtained for the smaller simulation cell in the following discussion.

We summarized in Table 1 the energetic and structural characteristics of the 576-atoms *a*-Si samples generated with the slowest cooling rates, along with data from other theoretical models. It can be seen that most atoms ($\sim 96 - 97\%$) are four-fold coordinated. In the case of WWW and BM models, all the atoms in the generated samples are four-fold coordinated. This percentage is reduced to 88 – 90% in conventional RMC models [25, 40], while it was increased to 96 – 99% in improved RMC models [26–28]. The percentage of fourfold-coordinated atoms is unrealistic for some RMC models [28, 41] and the paracrystalline models analyzed [43].

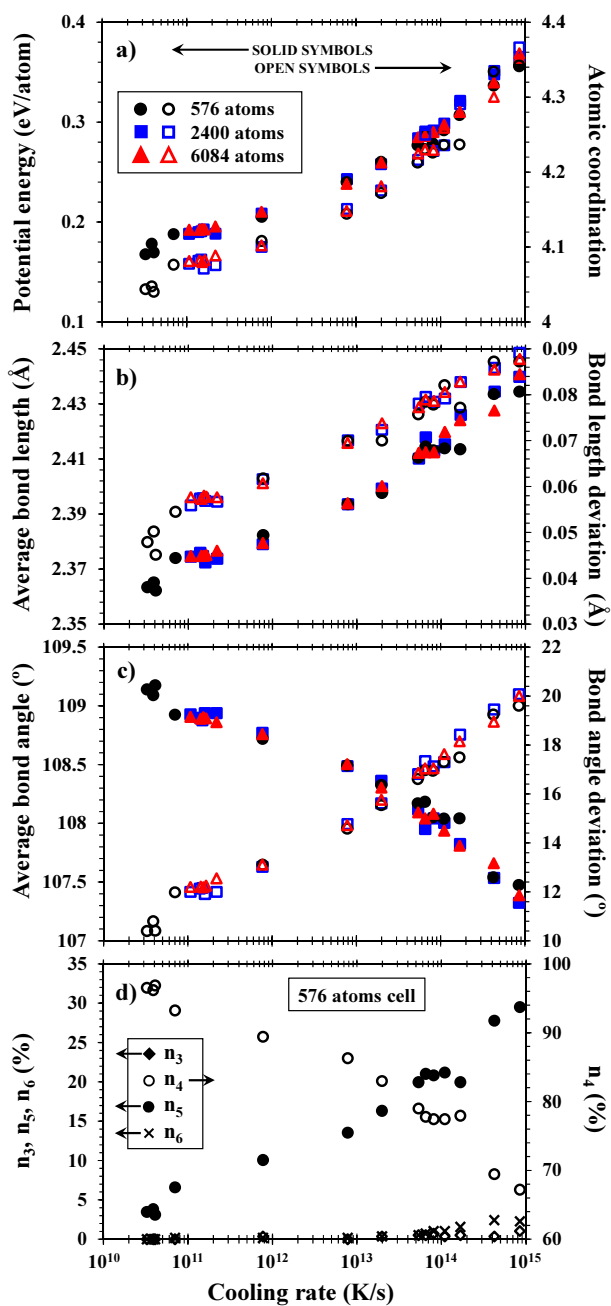


Figure 2: Energetic and structural characterization as a function of the cooling rate of samples equilibrated at 300 K after quenching: (a) atomic coordination and potential energy with respect to *c*-Si, (b) average bond length and its deviation, (c) average bond angle and its deviation, and (d) percentage of Si atoms with three (n_3), four (n_4), five (n_5) and six (n_6) Si neighbors. Only data from 576-atoms simulation cells was included in (d) for a better visualization as larger simulation cells follow the same trends as it happens in (a)-(c). Arrows indicate the axis of each data set.

Table 1: Structural and energetic characteristics of the 576-atoms *a*-Si samples obtained with the slowest cooling rates: potential energy with respect to *c*-Si, atomic coordination (At. coord.), percentage of Si atoms with three (n_3), four (n_4) and five (n_5) Si neighbors, average bond length (r_d) and its deviation ($\Delta\sigma$), and average bond angle (θ) and its deviation ($\Delta\theta$). Data from other computational models are also shown for comparison. Dash symbols indicate data unavailable in consulted references.

| | Quenching process | | | WWW ^a | BM ^b | RMC | | | | | Paracrystalline | | |
|--------------------|-------------------------------|-------|-------|------------------|-----------------|-----------|-------------------|---------------------|------------------|-----------|-----------------|---------------------|---------------------|
| | Cooling rate (10^{10} K/s) | | | | | Ref. [40] | Ref. [28] | | | Ref. [26] | Ref. [27] | MCRTDV ^f | MCXTDV ^g |
| | 4.1 | 3.9 | 3.3 | | | | SOAP ^c | INVERT ^d | RMC ^e | | | | |
| E_{pot} (eV/at.) | 0.17 | 0.18 | 0.17 | 0.217 | 0.264-0.304 | - | - | - | - | - | - | - | |
| At. coord. | 4.03 | 4.04 | 4.03 | 4 | 4 | 3.85 | 3.97 | 4.02 | 4.71 | 4 | - | 3.49 | 3.53 |
| n_3 (%) | 0 | 0 | 0 | 0 | 0 | - | 11.3 | 0 | 16.4 | 2 | - | 23.15 | 23.15 |
| n_4 (%) | 96.9 | 96.2 | 96.5 | 100 | 100 | 88 | 80.1 | 98 | 19.9 | 96 | 99.07 | 53.18 | 47.22 |
| n_5 (%) | 3.1 | 3.8 | 3.5 | 0 | 0 | - | 8.2 | 2 | 20.5 | 2 | - | 7.18 | 11.17 |
| r_d (Å) | 2.36 | 2.37 | 2.36 | 2.36 | 2.3 | - | 2.35 | 2.35 | 2.28 | - | - | 2.38 | 2.39 |
| $\Delta\sigma$ (Å) | 0.05 | 0.05 | 0.05 | 0.05 | 0.09-0.1 | - | 0.09 | 0.08 | 0.28 | - | - | 0.07 | 0.08 |
| θ (°) | 109.2 | 109.1 | 109.1 | 109.2 | 109.25-109.30 | 109.01 | 107.3 | 105.1 | 96.1 | 108.52 | 108.8 | 107.6 | 106.8 |
| $\Delta\theta$ (°) | 10.4 | 10.8 | 10.4 | 11 | 9.20-9.89 | 12.5 | 18.8 | 28.6 | 34.4 | 15.6 | 14.6 | 19.3 | 21.8 |

^aFrom Ref. [60]: WWW model relaxed with a tight-binding model. ^bFrom Refs. [32, 33]: BM models relaxed with Stillinger-Weber empirical potential. ^cFrom atomic positions of SOAP model in Ref. [28]. ^dFrom atomic positions of INVERT model in Ref. [28]. ^eFrom atomic positions of model in Ref. [28]. ^fFrom atomic positions of MCRTDV model in Ref. [43]. ^gFrom atomic positions of MCXTDV model in Ref. [43].

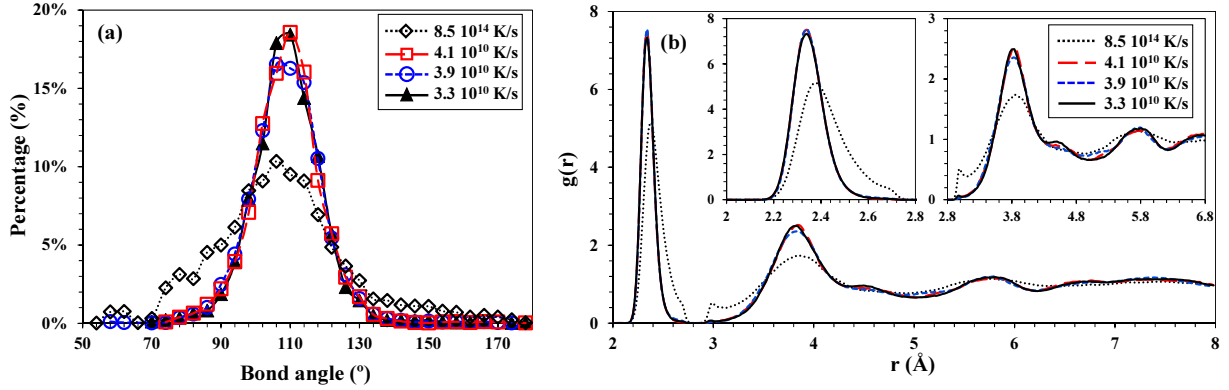


Figure 3: (a) Bond angle distribution, and (b) pair correlation function for the 576-atom *a*-Si samples generated with the fastest and the slowest cooling rates. Insets in (b) magnify selected regions of the pair correlation function for a better comparison.

Among the structural parameters of *a*-Si models, the bond angle deviation is a good indicator of the relaxation state of *a*-Si [61]. We represented in Fig. 3 the bond angle distributions of 576-atom *a*-Si samples generated with the fastest and the slowest cooling rates, along with their PCF. Slower cooling rates result in bond angle distributions with only one peak at the average bond angle reported in Table 1, and they do not show the typical peak at $\sim 60^\circ$ of *a*-Si samples generated with fast cooling rates. This peak is a signature of a supercooled liquid sample rather than an amorphous one [49]. For the case of the fastest cooling rates, i.e. $8.5 \cdot 10^{14}$ and $4.2 \cdot 10^{14}$ K/s, we analyzed the atomic coordination of atoms that presented bond angles between 50° and 70° . We found that on average 75% of those atoms are five-fold coordinated, 20% are six-fold coordinated, and 5% are four-fold coordinated. Thus, this peak corresponds to over-coordinated Si atoms [49]. It has been observed that *l*-Si undergoes structural and energetic changes when reducing the temperature, that makes its structure evolve towards the structure of *a*-Si through a glass transition [56, 59, 62–65]. Therefore, this phase transition cannot be completed when fast cooling rates are used, and over-coordinated atoms characteristic of *l*-Si remain in the sample.

Experiments show that relaxed *a*-Si has $\Delta\theta \sim 7 - 11^\circ$, while this value is increased in irradiated samples [11, 61]. In the case of theoretical models, WWW and BM models usually result in $\Delta\theta \sim 9 - 11^\circ$ [31–33], while RMC models tend to result in larger values as indicated in table 1 [26–28, 40]. Paracrystalline models included in Table 1 also present larger values for $\Delta\theta$. The quenching process is usually considered as an inappropriate method for generating *a*-Si since it results in large values of $\Delta\theta$ ($\Delta\theta = 14.6 - 17.6^\circ$ for 10^{13} K/s in Ref. [13], $\Delta\theta = 11.4 - 15.5^\circ$ for $2.3 \cdot 10^{13}$ K/s in Ref. [48], and $\Delta\theta = 20.2^\circ$ for $2.4 \cdot 10^{14}$ K/s in Ref. [27]). Nevertheless, we obtained bond angle deviations lower than 11° for cooling rates slower than 10^{11} K/s.

With respect to the PCFs shown in Fig. 3.b, the slowest cooling rates present similar PCFs, which are significantly different from the one of the sample generated with the fastest cooling rate. Slowest cooling rates results in a high and narrow peak at the bonding distance, wider peak at second-neighbor distance, empty region between first and second peaks, and oscillations around one for large distances [10, 49, 66]. Weak peaks at the sides of the empty region around 2.8 \AA that appear for the fastest cooling rate are known effects due to the cut-off function in the empirical potential [52]. These peaks are especially relevant in unrelaxed *a*-Si samples, while they are absent in well relaxed ones. There is a smooth evolution of characteristics of the PCF between curves shown in Fig. 3.b for the fastest and the slower cooling rates as the cooling rate is reduced (not shown).

In the following we will correlate the structural features of generated samples with experimental results in order to check the reliability of the MD quenching process for the generation of *a*-Si atomistic models. The

short range atomic structure of *a*-Si can be interpreted as a result of small deviations from the bond angle and the bond length of *c*-Si. In experimental works, bond angle and bond length deviations, along with the nearest neighbor distance (r_d), can be directly obtained from X-ray [9, 10] or neutron diffraction [66] measurements, while $\Delta\theta$ can be also evaluated indirectly from the TO-mode peak in Raman spectra [61]. Thus, the experimental range of $\Delta\theta$ and $\Delta\sigma$ determine the allowed dispersion range for bond angles and bond lengths in atomic models of *a*-Si, and it can be used to evaluate the validity of theoretically obtained atomistic structures.

We represented in Fig. 4 the correlation between the bond angle deviation ($\Delta\theta$), the relative bond length deviation with respect to the bonding distance of *c*-Si ($\Delta\sigma/r_0$), and the relative bond length difference with respect to *c*-Si ($\Delta r/r_0 = (r_d - r_0)/r_0$) of the samples generated in the present work, along with experimental data (*a*-Si generated by sputtering [7], CVD [8] and ion implantation [9]), and data from theoretical *a*-Si models (CRN models [67], WWW models [60], BM models [32, 33, 68, 69], RMC models [28], paracrystalline models [43], samples generated by quenching process [48], by bond defect accumulation [36], and by the accumulation of radiation induced damage [36]). We only included in Fig. 4 data from 576-atoms simulation cells for a clear visualization of the figure, as data from larger simulation cells overlap the smaller simulation cell points.

Data from experiments in Fig. 4 indicate that $\Delta\theta \sim 7 - 11.5^\circ$, $\Delta\sigma/r_0 \sim 1.3 - 2.1\%$, and $\Delta r/r_0 \sim 0 - 0.9\%$. Although no data of laser-quenched *a*-Si experimental samples was included in Fig. 4 (these data was not available in consulted references), it was found that this type of *a*-Si is structurally very similar to *a*-Si generated by CVD [5, 15, 17]. Thus, the structural characteristics of laser-quenched *a*-Si are expected to be very similar to those of CVD samples shown in Fig. 4, and laying inside the range for $\Delta\theta$, $\Delta\sigma/r_0$, and $\Delta r/r_0$ previously indicated. Samples generated in the present work approach the region of experimental data as the cooling rate is reduced. In particular, samples generated with cooling rates below 10^{11} K/s (whose characteristics were described in Table 1 and Fig. 2) present structural parameters in the range of experimental data. We also performed quenching simulations using the Stillinger-Weber potential [70] for simulation cells with 576 and 2400 atoms (not shown in Fig. 4). The best structural parameters obtained for these simulations were $\Delta\theta \sim 15^\circ$, $\Delta\sigma/r_0 \sim 4.2\%$, and $\Delta r/r_0 \sim 2.6\%$, which are far from the experimental range.

In the case of first computer generated CRN models [67], structures are relaxed with the Keating potential [71]. This potential is usually employed for evaluating the elastic strain in atomic structural models from bond bending and bond stretching contributions. Most of considered CRN models lay within the region of experimental data, except for a couple of points. The one with the largest bond length deviation in Fig.4.b correspond to a model initially constructed for amorphous SiO_2 , where O atoms were removed before relaxation. Thus, the relaxed structure kept some features of the initial amorphous SiO_2 structure as indicated in Ref. [67].

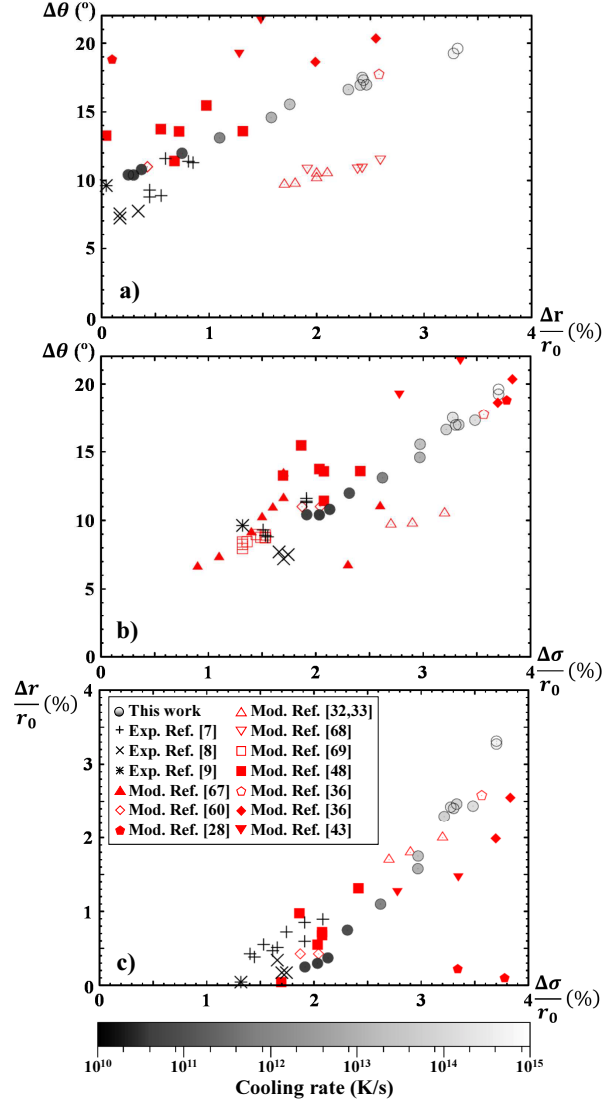


Figure 4: Correlation between the bond angle deviation ($\Delta\theta$), the relative bond length deviation with respect to *c*-Si ($\Delta\sigma/r_0$), and the relative bond length difference with respect to *c*-Si ($\Delta r/r_0$). Data of present work from 576-atoms simulation cells is represented by circles \circ whose filling color refers to the cooling rate used as indicated by the gray scale at the bottom of the figure. Black symbols are for experimental *a*-Si generated by sputtering (black + symbols [7]), CVD (black \times symbols [8]) and ion implantation (black * symbol [9]). CVD and sputtering samples were characterized at room temperature, and implanted sample at 10 K. Red symbols are for *a*-Si models (Mod.) generated theoretically, including first computer generated CRN models (red \blacktriangle symbols [67]), WWW models (red \diamond symbols [60]), BM models (red \triangle [32, 33], ∇ [68], and \square [69] symbols), RMC models (red \blacklozenge symbols for INVERT and SOAP structures of Ref. [28]), paracrystalline models (red \blacktriangledown symbols [43]), and *a*-Si samples from quenching process with cooling rates of $2.3 \cdot 10^{13}$ K/s (red \blacksquare symbols [48]), from the accumulation of bond defects (red \blacklozenge symbols [36]), and from the accumulation of damage generated by recoils (red \diamond symbols [36]). CRN, WWW, BM and RMC models are characterized at 0 K. Samples of the present work and those of Refs. [36, 48] are characterized at 300 K.

In the case of the WWW model [60], it was relaxed using a tight-binding model. It lays within the region of experimental data, and a subsequent annealing results in a slight reduction of Δr (not shown in Fig. 4). BM models present larger values of $\Delta\sigma/r_0$ and $\Delta r/r_0$ [32, 33, 68] than experimental data, which increase upon irradiation and decrease with a subsequent thermal annealing [68]. When volume relaxation is allowed in the simulation cell [69], the structural parameters lay within the experimental range as observed in Fig. 4.b. Nevertheless, Zotov *et al.* employed a Kirkwood-type harmonic potential for the relaxation step, which is based on bond bending and bond stretching as the Keating potential [72], while the other BM models shown in Fig. 4 are relaxed using Stillinger-Weber empirical potential [32, 33, 68]. This difference in the empirical potential used for relaxing the generated *a*-Si structure might originate the difference in $\Delta\sigma/r_0$ between BM models observed in Fig. 4.b.

Available data from RMC models [28] show low values of $\Delta r/r_0$ than $\Delta\sigma/r_0$, while $\Delta\theta$ is larger than experimental values. Values of $\Delta\theta$ reported in table 1 are also larger than those found in experimental samples. This comparison seems to indicate that RMC models could be improved if angular information from experiments was also considered in the fitting process for the generation of the atomic structures. The paracrystalline models included in Fig. 4 present values for $\Delta r/r_0$, $\Delta\sigma/r_0$, and $\Delta\theta$ larger than experimental data [43].

Quenched samples reported by other works [48] present angular deviations larger than the experimental samples, and in agreement with values of $\Delta\theta$ for equivalent cooling rates in the present work ($\sim 2 \cdot 10^{13}$ K/s). Those samples were generated using with *ab initio* simulations, and the cooling rate used was limited by the computational cost of the simulation technique. Finally, samples generated from the accumulation of bond defects [36] and from the accumulation of damage generated by recoils [36] result in values of $\Delta\theta$, $\Delta\sigma/r_0$ and $\Delta r/r_0$ larger than the range of experimental data.

In order to elucidate whether the generated *a*-Si samples had a random or a paracrystalline structure, we evaluated the spatial distribution of four-fold coordinated Si atoms with dihedral angles of $180^\circ \pm 4^\circ$ of samples generated with cooling rates slower than 10^{11} K/s, as in Ref. [46]. We found that they were randomly distributed in the simulation cell rather than grouped in crystalline grains. In the case of samples crystallized during the quenching process, we represented in Fig. 5 their PCF, along with the PCF for *c*-Si at 300 K and for *a*-Si generated with $4.1 \cdot 10^{10}$ K/s cooling rate. It can be seen from Fig. 5 that the PCF of crystallized samples is closer to the one of *c*-Si than to the one of *a*-Si. Thus, these samples do not correspond to paracrystalline *a*-Si structures.

Thermal annealing is commonly used to reduce the defect concentration and to relax the generated *a*-Si samples, both experimentally [5, 9–13] and computationally [50, 60, 68]. We analyzed how subsequent long

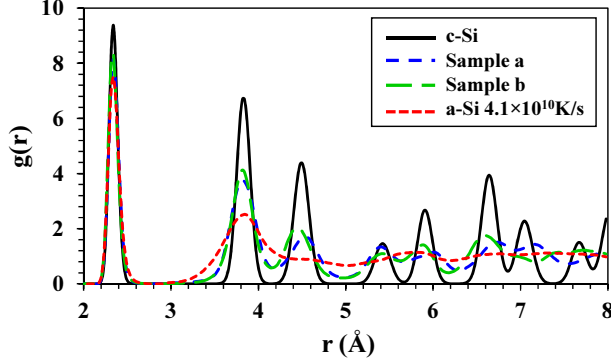


Figure 5: Pair correlation function of crystallized samples. The pair correlation function for *c*-Si at 300 K and for the *a*-Si generated with a cooling rate of $4.1 \cdot 10^{10}$ K/s are also shown for comparison.

annealing simulations (from 0.75 to 0.95 μ s) modify the structural features of computationally generated *a*-Si samples. For this purpose, we selected the 576-atoms sample obtained with a cooling rate of $4.1 \cdot 10^{10}$ K/s (with $\Delta\theta = 10.4^\circ$, $\Delta\sigma/r_0 = 1.9\%$ and $\Delta r/r_0 = 0.25\%$ before annealing) as a representative example of highly relaxed computer generated *a*-Si. As examples for unrelaxed *a*-Si samples, we considered the 576-atoms sample generated with a cooling rate of $8.1 \cdot 10^{13}$ K/s (with $\Delta\theta = 17^\circ$, $\Delta\sigma/r_0 = 3.3\%$ and $\Delta r/r_0 = 2.4\%$ before annealing), and a sample from a previous work generated by the accumulation of the damage generate by recoils (with $\Delta\theta = 17.7^\circ$, $\Delta\sigma/r_0 = 3.6\%$ and $\Delta r/r_0 = 2.6\%$ before annealing) [36]. Finally, we considered *a*-Si samples generated in a previous work by the accumulation of 30% (with $\Delta\theta = 18.6^\circ$, $\Delta\sigma/r_0 = 3.7\%$ and $\Delta r/r_0 = 2\%$ before annealing) and 45% (with $\Delta\theta = 20.3^\circ$, $\Delta\sigma/r_0 = 3.8\%$ and $\Delta r/r_0 = 2.55\%$ before annealing) of bond defects as cases for highly unrelaxed computer generated *a*-Si [36].

We represented in Fig. 6 the evolution of the potential energy of 576-atoms *a*-Si samples during annealing simulations at 900 K and 1300 K with respect to *c*-Si at the same temperature. It can be seen that the *a*-Si sample generated with the slower cooling rate (SCR) do not significantly change its energy during annealing, while the potential energy of the other samples is reduced. In addition, initial differences in the potential energy between unrelaxed samples are appreciably reduced after some time ($\sim 10^3$ ps for 900 K and $\sim 10^2$ ps for 1300 K). Afterwards, the potential energy evolution of unrelaxed samples is similar. In the case of 1300 K, the simulated time is long enough for unrelaxed samples to reach the relaxation state of SCR sample after $\sim 10^2$ ns at 1300 K, while their potential energy is still ~ 0.03 eV/atom over the SCR sample after annealing at 900K. Longer annealing times would be required to reach the relaxation state of SCR sample at 900 K.

We summarized in Fig. 7 the values $\Delta\theta$, $\Delta\sigma/r_0$, and $\Delta r/r_0$ of samples at the end of long annealing simulations

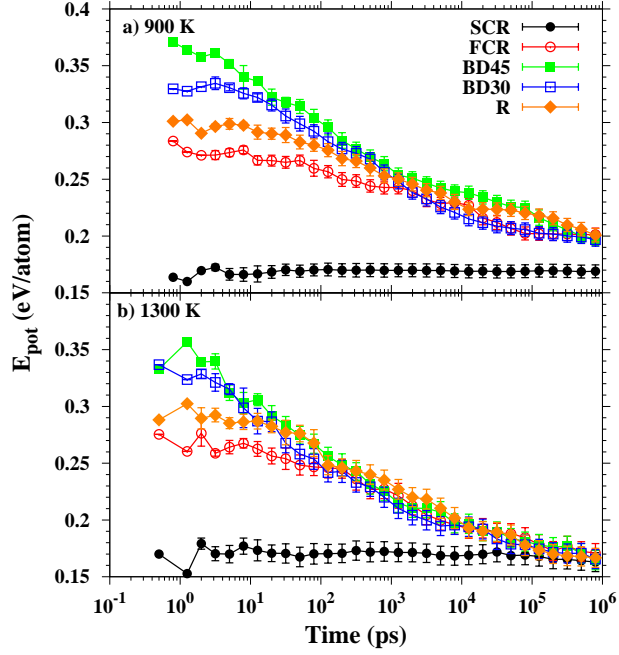


Figure 6: Potential energy of selected 576-atoms *a*-Si samples during long annealing simulations at (a) 900 K and (b) 1300 K with respect to *c*-Si at the same temperature. SCR and FRC stands for 576-atoms *a*-Si samples generated with a slow ($4.1 \cdot 10^{10}$ K/s) and fast ($8.1 \cdot 10^{13}$ K/s) cooling rate, respectively; BD45 and BD30 stands for *a*-Si samples generated by the accumulation of a 45% and 30% concentration of bond defects, respectively; and R stands for the *a*-Si sample generated by the accumulation of damage generated by recoils. To reduce data noise, we considered 5 intervals per decade, and we averaged data within each interval. Error bars show the standard deviation of averages. Initial intervals include fewer points and their standard deviation is not appreciable.

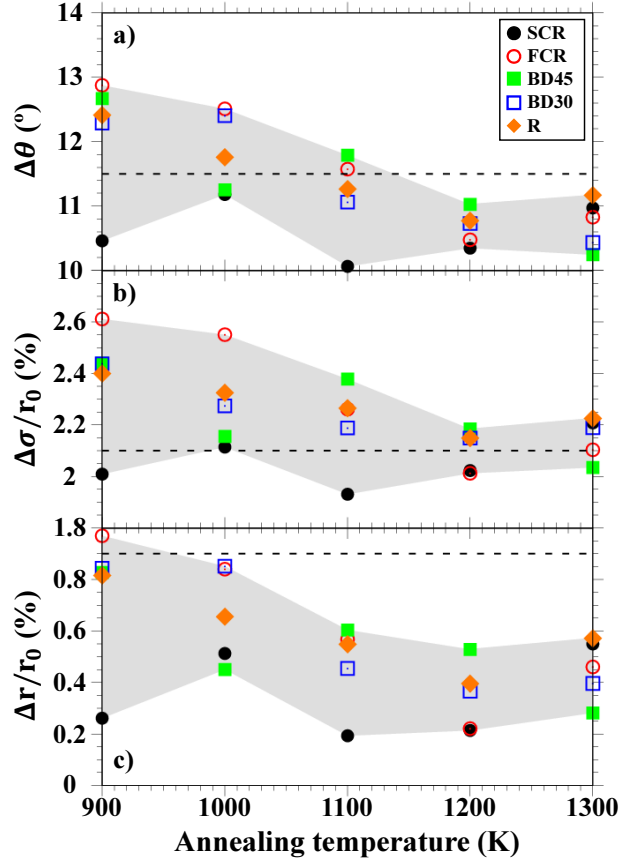


Figure 7: (a) Bond angle deviation ($\Delta\theta$), (b) relative bond length deviation with respect to *c*-Si ($\Delta\sigma/r_0$), and (c) relative bond length difference with respect to *c*-Si ($\Delta r/r_0$) as a function of temperature of samples at the end of long annealing simulations equilibrated at 300 K. Labels are as in Fig. 6. Horizontal dashed line indicates the upper limit of experimental data. Shaded areas are to guide the eye.

and subsequently equilibrated at 300 K. The comparison of $\Delta\theta$, $\Delta\sigma/r_0$, and $\Delta r/r_0$ values before and after annealing indicates that the performed annealing is quite effective in relaxing the samples except for the SCR sample. The structural features of the SCR sample vary around the values obtained after quenching. Thus, this sample is not further relaxed after the annealing conditions considered, as it was also inferred from Fig. 6. In the case of the other samples, the reduction of $\Delta\theta$, $\Delta\sigma/r_0$, and $\Delta r/r_0$ is larger as the annealing temperature increases. In the case of 900 K, the small energy difference of samples with respect to the SCR sample at the end of the annealing simulation pointed out in Fig. 6.a results in values of $\Delta\theta$ and $\Delta\sigma/r_0$ above the experimental upper limit. Thus, even 1 μ s annealing step at 900 K was not enough to reduce the variability range of these structural parameters within the experimental range. For annealing temperatures above 1100 K, $\Delta\theta$ lays below the upper limit of experimental values in all cases, and values of $\Delta\sigma/r_0$ oscillates around the upper limit of the experimental range. Thus, the annealing time considered is long enough for temperatures above 1100 K. For $\Delta r/r_0$, almost all points are within the experimental range after annealing, and for annealing temperatures above 1100 K they are below 0.6%. In addition, the dispersion in the structural parameters represented in Fig. 7, which has been schematically indicated by the shadowed areas, is reduced as the annealing temperature increases. Any initial structural difference among samples is negligible after a microsecond annealing at temperatures above 1200 K, i.e. *a*-Si samples tend to equivalent relaxed structures upon convenient annealing.

4. Conclusions

We reviewed the viability of the quenching process for generating realistic *a*-Si samples using classical molecular dynamics simulations. For this purpose, we considered cooling rates ranging from $8.5 \cdot 10^{14}$ to $3.3 \cdot 10^{10}$ K/s. Crystallization of samples was observed for slower cooling rates. We analyzed the structural characteristics of generated samples, and we compared the obtained results with data available in the literature from experiments and from other theoretical structural models.

By comparing the bond length and angle parameters in the generated *a*-Si samples with experimental and other theoretical data, we could determine the conditions under which the quenching process results in *a*-Si samples within the variability range of experimental samples. We found that *a*-Si samples generated in the present work approach to the range of structural parameters found in experimental samples as the cooling rate is reduced. In particular, cooling rates below 10^{11} K/s resulted in samples with structural parameters in the range of experimental data. Equivalent results have been obtained recently using more sophisticated Machine-Learning-Driven molecular dynamics simulations [51]. These cooling rates, that are quite slow from

a computational point of view, are experimentally achieved by pulsed energy melting techniques. Thus, care should be taken when using faster cooling rates as the obtained *a*-Si structures might not be realistic.

We also evaluated the possibility of further relaxing the generated *a*-Si samples by means of long annealing simulations. We found that microsecond annealings above 1100 K can result in structural parameters within the experimental range for initially unrelaxed samples. Lower temperatures would require annealing times longer than 1 microsecond. However, the structure of initially well relaxed *a*-Si samples is not significantly modified during annealing.

Being *a*-Si an amorphous material, there is not a unique atomistic configuration describing its structure. Nevertheless, computer generated models should provide atomic structures in good agreement with experimental data. Although there exist sophisticated state-of-the-art algorithms that adequately produce *a*-Si atomistic models, we showed that the simpler quenching process can also result in realistic *a*-Si samples whenever the cooling used is below 10^{11} K/s. These slow cooling rates are not longer a limitation for computational resources available nowadays. The simulation with the slower cooling rate considered for the 576-atoms simulation cell took 26.5 hours in a single processor in a Intel Xeon E5620 working at 2.4 GHz, time that can be reduced using parallelization. Thus, the quenching process can be considered a proper method for generating structural models of *a*-Si that resembles pulsed energy melting techniques. Although we used empirical potentials in our simulations, generated samples could be used as the input configuration of more fundamental techniques (tight-binding or *ab initio*) for refinement (as it was done in Ref. [60]) to overcome the computational cost of carrying out the quenching process with them. In addition, subsequent annealing simulations are not necessary for initially well relaxed samples. Thus, it is preferable to generate *a*-Si samples as relaxed as possible rather than using subsequent annealing simulations for their further relaxation, as they would require annealing simulations of the order of μ s that are computationally time demanding.

Acknowledgement

I.S. thanks helpful suggestions and data from Dr. Masatoshi Wakagi. This work has been supported by EU (FEDER) funds from the Spanish Ministerio de Ciencia e Innovación under Projects No. TEC2014-60694-P and TEC2017-86150-P, and from the Junta de Castilla y León under Projects No. VA097P17 and VA119G18.

References

- [1] H. Sai, T. Matsui, K. Matsubara, Appl. Phys. Lett. 109 (2016) 183506.

- [2] M. Canino, G. Regula, M. Xu, E. Ntzoenzok, B. Pichaud, *Mat. Sci. Eng. B* 159 (2009) 338.
- [3] M. Aboy, L. Pelaz, E. Bruno, S. Mirabella, S. Boninelli, *J. Appl. Phys.* 110 (2011) 073524.
- [4] P. Shufflebotham, H. Card, A. Thanailakis, *J. Non-Cryst. Solids* 92 (1987) 183.
- [5] S. Roorda, W. C. Sinke, J. M. Poate, D. C. Jacobson, S. Dierker, B. S. Dennis, D. J. Eaglesham, F. Spaepen, P. Fuoss, *Phys. Rev. B* 44 (1991) 3702.
- [6] R. Zallen, *The Physics of Amorphous Solids*, Wiley-VCH Verlag GmbH, 2007.
- [7] M. Wakagi, K. Ogata, A. Nakano, *Phys. Rev. B* 50 (1994) 10666.
- [8] M. Wakagi, Ph.D. thesis, Tokyo Institute of Technology. (1995). doi:10.11501/3116547.
- [9] K. Laaziri, S. Kycia, S. Roorda, M. Chicoine, J. L. Robertson, J. Wang, S. C. Moss, *Phys. Rev. B* 60 (1999) 13520.
- [10] K. Laaziri, S. Kycia, S. Roorda, M. Chicoine, J. L. Robertson, J. Wang, S. C. Moss, *Phys. Rev. Lett.* 82 (1999) 3460.
- [11] P. A. Stolk, F. W. Saris, A. J. M. Berntsen, W. F. van der Weg, L. T. Sealy, R. C. Barklie, G. Krötz, G. Müller, *J. Appl. Phys.* 75 (1994) 7266.
- [12] L. Pelaz, L. A. Marqués, J. Barbolla, *J. Appl. Phys.* 96 (11) (2004) 5947.
- [13] E. Holmström, B. Haberl, O. Pakarinen, K. Nordlund, F. Djurabekova, R. Arenal, J. Williams, J. Bradby, T. Petersen, A. Liu, *J. Non-Cryst. Solids* 438 (2016) 26.
- [14] R. Tsu, R. T. Hodgson, T. Y. Tan, J. E. Baglin, *Phys. Rev. Lett.* 42 (1979) 1356.
- [15] N. Maley, J. S. Lannin, A. G. Cullis, *Phys. Rev. Lett.* 53 (1984) 1571.
- [16] M. O. Thompson, J. W. Mayer, A. G. Cullis, H. C. Webber, N. G. Chew, J. M. Poate, D. C. Jacobson, *Phys. Rev. Lett.* 50 (1983) 896.
- [17] J. S. Custer, M. O. Thompson, P. H. Bucksbaum, *Appl. Phys. Lett.* 53 (1988) 1402.
- [18] K. Weiser, *Prog. Solid State Chem.* 11 (1976) 403.

- [19] P. A. Stolk, L. Calcagnile, S. Roorda, W. C. Sinke, A. J. M. Berntsen, W. F. van der Weg, *Appl. Phys. Lett.* 60 (1992) 1688.
- [20] M. Stutzmann, W. B. Jackson, C. C. Tsai, *Phys. Rev. B* 32 (1985) 23.
- [21] S. Mirabella, D. De Salvador, E. Bruno, E. Napolitani, E. F. Pecora, S. Boninelli, F. Priolo, *Phys. Rev. Lett.* 100 (2008) 155901.
- [22] E. Johlin, C. B. Simmons, T. Buonassisi, J. C. Grossman, *Phys. Rev. B* 90 (2014) 104103.
- [23] D. Drabold, T. Abtew, *Defects in Amorphous Semiconductors: Amorphous Silicon*, Springer Berlin Heidelberg, Berlin, Heidelberg, 2007, p. 245.
- [24] M. H. Brodsky, *J. Vac. Sci. Technol.* 8 (1971) 125.
- [25] A. Pandey, P. Biswas, D. A. Drabold, *Phys. Rev. B* 92 (2015) 155205.
- [26] A. Pandey, P. Biswas, B. Bhattarai, D. A. Drabold, *Phys. Rev. B* 94 (2016) 235208.
- [27] A. Pandey, P. Biswas, D. A. Drabold, *Sci. Rep.* 6 (2016) 33731.
- [28] M. J. Cliffe, A. P. Bartók, R. N. Kerber, C. P. Grey, G. Csányi, A. L. Goodwin, *Phys. Rev. B* 95 (2017) 224108.
- [29] D. Igram, B. Bhattarai, P. Biswas, D. Drabold, *J. Non-Cryst. Solids* 492 (2018) 27.
- [30] W. H. Zachariasen, *J. Am. Chem. Soc.* 54 (1932) 3841.
- [31] F. Wooten, K. Winer, D. Weaire, *Phys. Rev. Lett.* 54 (1985) 1392.
- [32] G. T. Barkema, N. Mousseau, *Phys. Rev. B* 62 (2000) 4985.
- [33] R. L. C. Vink, G. T. Barkema, M. A. Stijnman, R. H. Bisseling, *Phys. Rev. B* 64 (2001) 245214.
- [34] L. A. Marqués, L. Pelaz, J. Hernández, J. Barbolla, G. H. Gilmer, *Phys. Rev. B* 64 (2001) 045214.
- [35] L. A. Marqués, L. Pelaz, M. Aboy, L. Enríquez, J. Barbolla, *Phys. Rev. Lett.* 91 (2003) 135504.
- [36] I. Santos, P. López, M. Aboy, L. A. Marqués, L. Pelaz, Characterization of amorphous si generated through classical molecular dynamics simulations, in: 2017 Spanish Conference on Electron Devices (CDE), 2017, pp. 1–4. doi:10.1109/CDE.2017.7905213.

- [37] R. L. McGreevy, L. Pusztai, *Mol. Simul.* 1 (1988) 359.
- [38] O. Gereben, L. Pusztai, *Phys. Rev. B* 50 (1994) 14136.
- [39] R. L. McGreevy, *J. Phys.: Condens. Matter* 13 (2001) R877.
- [40] P. Biswas, R. Atta-Fynn, D. A. Drabold, *Phys. Rev. B* 69 (2004) 195207.
- [41] M. J. Cliffe, M. T. Dove, D. A. Drabold, A. L. Goodwin, *Phys. Rev. Lett.* 104 (2010) 125501.
- [42] S. M. Nakhmanson, P. M. Voyles, N. Mousseau, G. T. Barkema, D. A. Drabold, *Phys. Rev. B* 63 (2001) 235207.
- [43] M. M. J. Treacy, K. B. Borisenko, *Science* 335 (2012) 950.
- [44] S. Roorda, L. J. Lewis, *Science* 338 (2012) 1539–b.
- [45] M. M. J. Treacy, K. B. Borisenko, *Science* 338 (2012) 1539–c.
- [46] J. Gibson, M. Treacy, *Ultramicroscopy* 176 (2017) 74.
- [47] S. Izumi, S. Hara, T. Kumagai, S. Sakai, *Comput. Mater. Sci.* 31 (2004) 258.
- [48] K. Jarolimek, R. A. de Groot, G. A. de Wijs, M. Zeman, *Phys. Rev. B* 79 (2009) 155206.
- [49] M. Ishimaru, S. Fig05Fig05 Munetoh, T. Motooka, *Phys. Rev. B* 56 (1997) 15133.
- [50] D. Choudhary, P. Clancy, *J. Chem. Phys.* 122 (2005) 174509.
- [51] V. L. Deringer, N. Bernstein, A. P. Bartk, M. J. Cliffe, R. N. Kerber, L. E. Marbella, C. P. Grey, S. R. Elliott, G. Csny, *J. Phys. Chem. Lett.* 9 (2018) 2879.
- [52] J. Tersoff, *Phys. Rev. B* 38 (1988) 9902.
- [53] L. A. Marqués, L. Pelaz, P. Castrillo, J. Barbolla, *Phys. Rev. B* 71 (2005) 085204.
- [54] K. J. Dudeck, L. A. Marqués, A. P. Knights, R. M. Gwilliam, G. A. Botton, *Phys. Rev. Lett.* 110 (2013) 166102.
- [55] L. A. Marqués, M. Aboy, K. J. Dudeck, G. A. Botton, A. P. Knights, R. M. Gwilliam, *J. Appl. Phys.* 115 (2014) 143514.

- [56] L. A. Marqués, L. Pelaz, M. Aboy, J. Barbolla, Nucl. Instrum. Methods Phys. Res. B 216 (2004) 57.
- [57] J. K. Bording, J. Taftø, Phys. Rev. B 62 (2000) 8098.
- [58] M. Ishimaru, S. Munetoh, T. Motooka, K. Moriguchi, A. Shintani, Phys. Rev. B 58 (1998) 12583.
- [59] S. J. Cook, P. Clancy, Phys. Rev. B 47 (1993) 7686.
- [60] N. Bernstein, J. L. Feldman, M. Fornari, Phys. Rev. B 74 (2006) 205202.
- [61] P. Roura, J. Farjas, P. R. i Cabarrocas, J. Appl. Phys. 104 (2008) 073521.
- [62] S. Sastry, C. Austen Angell, Nature Materials 2 (2003) 739.
- [63] P. Ganesh, M. Widom, Phys. Rev. Lett. 102 (2009) 075701.
- [64] A. Hedler, S. L. Klaumünzer, W. Wesch, Nature Materials 3 (2004) 804.
- [65] M. Beye, F. Sorgenfrei, W. F. Schlotter, W. Wurth, A. Föhlisch, Proceedings of the National Academy of Sciences 107 (39) (2010) 16772.
- [66] J. Fortner, J. S. Lannin, Phys. Rev. B 39 (1989) 5527.
- [67] D. Beeman, R. Tsu, M. F. Thorpe, Phys. Rev. B 32 (1985) 874.
- [68] P. Dagenais, L. J. Lewis, S. Roorda, J. Phys. Cond. Matter 27 (2015) 295801.
- [69] N. Zotov, M. Marinov, N. Mousseau, G. Barkema, J. Phys. Cond. Matter 11 (1999) 9647.
- [70] F. H. Stillinger, T. A. Weber, Phys. Rev. B 31 (1985) 5262.
- [71] P. N. Keating, Phys. Rev. 145 (1966) 637.
- [72] J. G. Kirkwood, J. Chem. Phys. 7 (1939) 506.